# Observation of near-field correlations in spontaneous parametric down-conversion

H. Di Lorenzo Pires[*] and M. P. van Exter[†]

*Huygens Laboratory, Leiden University, P.O. Box 9504, 2300 RA Leiden, The Netherlands*

(Received 9 July 2008; published 3 April 2009)

We experimentally demonstrate how the two-photon field generated by spontaneous parametric down-conversion contains an intriguing fine structure associated with the positional spread within the photon pair. The obtained results provide a three-dimensional picture of the near-field correlations, which are determined by the phase-matching conditions. These correlations are compared with previous results on second-harmonic generation, spatial antibunching, and transverse entanglement in parametric down-conversion.

Spatial entanglement between photons can be easily generated in spontaneous parametric down-conversion (SPDC), where a single pump photon splits into a pair of down-converted photons [1]. These nonclassical correlations have been essential in many landmark experiments on quantum entanglement, such as ghost interference [2], quantum lithography [3,4], and recent demonstration of Bell inequalities with spatially entangled modes [5]. Having a wide range of applications, full knowledge of the spatial properties of the SPDC field is highly desirable.

Spatial correlations in any coherent two-photon field naturally occur on two length scales, being the spread in the "center of mass" of the photon pair and the "positional spread" within each pair. Most experiments operate in a regime where the first length scale, which is set by the width of the pump laser, is much larger than the structure that originates from the phase-matching condition of the pair creation. This "fine structure" is then generally removed and conveniently replaced by a $\delta$ function in position and a uniform angular emission [6]. In this so-called thin-crystal limit, spatial entanglement boils down to the statement that the two-photon field contains a copy of the pump profile. We will go beyond this simplified approach.

This Rapid Communication describes the experimental observation of a rich structure in the two-photon field that is associated with the spatial correlations originated from the phase-matching conditions. Apart from its intrinsic value, the obtained results provide a link with prior experiments on second-harmonic generation (SHG) [7,8], spatial antibunching of photons [9,10], and measurements on two-photon position-momenta correlations [11,12]. Furthermore, some consequences of the observed structures to the spatial entanglement will be addressed.

In the absence of walk-off, the two-photon wave function in momentum representation has a special form, factorizing in two functions of the sum and difference transverse momenta as [6,13]

$$\widetilde{A}(\boldsymbol{q}_1, \boldsymbol{q}_2) = \widetilde{E}_p(\boldsymbol{q}_1 + \boldsymbol{q}_2)\widetilde{V}(\boldsymbol{q}_1 - \boldsymbol{q}_2), \tag{1}$$

where $\widetilde{E}_p(\boldsymbol{q})$ is the angular spectrum of the pump beam and $\widetilde{V}(\boldsymbol{q}) = \mathrm{sinc}(b^2|\boldsymbol{q}|^2 + \varphi)$ derives from the phase-matching con-

*pires@molphys.leidenuniv.nl
†mvexter@molphys.leidenuniv.nl

ditions, with $b^2 = L/8n_o k$. $L$ is the crystal thickness, $k$ is the down-converted field wave vector, $n_o$ is the refractive index at the down-converted frequency, and $\varphi$ is the phase-mismatch parameter, which accounts for operation outside perfect phase matching. These momentum correlations can be measured in the far field, where each plane wave in the angular spectrum contributes to the field at a defined point. In that regime the "sinc" function, originated from the phase-matching conditions, is generally much wider than the pump profile $\widetilde{E}_p$ and is often neglected in the analysis. We are interested, instead, in the near-field regime. There the opposite is true and the spatial representation of the phase-matching function shapes the position correlations within the photon pairs.

The problem can be analyzed considering the ideal imaging system (with unity magnification) depicted in the inset of Fig. 1. The probability amplitude of detecting two-photon coincidences at the image plane ($z=0$) is given by the Fourier transform of Eq. (1), which links transverse momenta $\boldsymbol{q}$ to transverse coordinates $\boldsymbol{\rho}$. In the vicinity of $z=0$, which corresponds to an image of the center of the crystal, the two-photon correlation assumes the form

$$A(\boldsymbol{\rho}_1, \boldsymbol{\rho}_2; z) = \int\!\!\!\int_{-\infty}^{+\infty} d\boldsymbol{q}_1 d\boldsymbol{q}_2 \widetilde{A}(\boldsymbol{q}_1, \boldsymbol{q}_2) \exp\left(-i\frac{q_1^2 + q_2^2}{2k}z\right)$$
$$\times \exp(-i\boldsymbol{q}_1 \cdot \boldsymbol{\rho}_1 - i\boldsymbol{q}_2 \cdot \boldsymbol{\rho}_2), \tag{2}$$

where the first exponential accounts for the field propagation around the image plane and the second one is the Fourier kernel. It should be stressed that the plane $z=0$ contains contribution from all points inside the crystal and behaves as a secondary light source. Equation (2) also factorizes in two functions of the sum and difference coordinates $A(\boldsymbol{\rho}_1, \boldsymbol{\rho}_2; z) = E_p(\frac{\boldsymbol{\rho}_1 + \boldsymbol{\rho}_2}{2}; z)V(\boldsymbol{\rho}_1 - \boldsymbol{\rho}_2; z)$. It is straightforward to show that for a wide pump beam the two-photon field depends dominantly on the difference coordinate $\boldsymbol{\rho}_- = \boldsymbol{\rho}_1 - \boldsymbol{\rho}_2$ in the image plane,

$$V(\boldsymbol{\rho}_-; z) \propto \int_{-\infty}^{+\infty} d\boldsymbol{q}\, \widetilde{V}(2\boldsymbol{q}) \exp\left(-i\frac{|\boldsymbol{q}|^2}{k}z - i\boldsymbol{q} \cdot \boldsymbol{\rho}_-\right). \tag{3}$$

The coincidence counting rate measured by pointlike detectors placed in transverse positions $\boldsymbol{\rho}_1$ and $\boldsymbol{\rho}_2$ at plane $z$ is then $R_{cc} \propto |V(\boldsymbol{\rho}_-; z)|^2$.

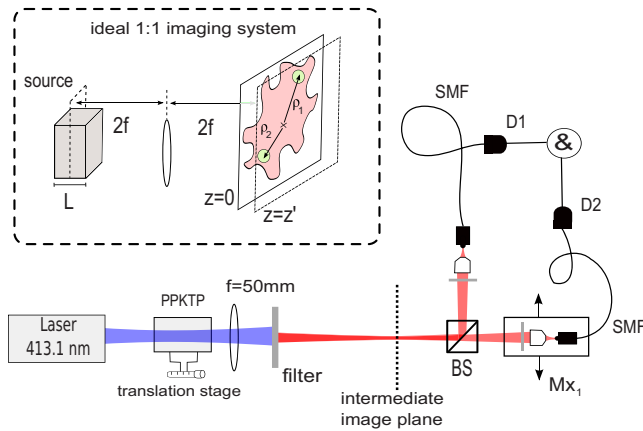A more realistic description must take into account the

FIG. 1. (Color online) Experimental setup for measuring the near-field correlations in the two-photon field. The inset shows an ideal 1:1 imaging system, where $z=0$ is defined as the image plane with respect to the center of the crystal. We are interested in probing the spatial correlations in the vicinity of the image plane. The inset also illustrates how the finite resolution of the detectors should be included in the description. In our experimental implementation we use a $13\times$ magnified imaging system. Spatially entangled photon pairs generated in PPKTP are separated at a beam splitter, selected with filters (spectral width 5 @ 826 nm) and detected by photon counters and coincidence electronics (D1 and D2). Only coincidence counts within a time window of 1.4 ns are considered. The crystal position can be adjusted by a translation stage. An $f =50$ mm lens is used to make a $13\times$ magnified image of the near field onto an intermediate plane, which is then imaged onto single-mode optical fibers by objective lenses. It is important to remark that all transverse planes inside the crystal contribute coherently to this "image."

finite resolution of the detectors. Working with single-mode (fiber-coupled) detectors centered at $\boldsymbol{\rho}_1$ and $\boldsymbol{\rho}_2$, the measured two-photon field will then be given by an overlap integral of the generated field and the Gaussian profile $\phi$ of the detection modes,

$$V_{\text{project}}(\boldsymbol{\rho}_-;z) \propto V * \phi(\boldsymbol{\rho}_1) * \phi(\boldsymbol{\rho}_2), \tag{4}$$

where $*$ denotes the convolution integral. Using compact detection modes, the thus obtained projected two-photon field

will closely resemble the generated field $V(\boldsymbol{\rho}_-;z)$ and can be regarded as a smoothed version thereof.

Figure 1 shows the experimental setup used to observe the near-field structure in the two-photon field. In our experimental implementation we use a magnified (instead of a 1:1) imaging system. Entangled photon pairs of equal polarization are generated by mildly focusing ($w_p=157$ $\mu$m) a laser beam ($\lambda_p=413.1$ nm) on a $L=5$-mm-thick periodically poled potassium titanyl phosphate (PPKTP) crystal, whose transverse dimensions are much larger than the pump width. The refractive index $n=1.843$ for PPKTP at $\lambda_0=826.2$ nm and $T\approx60$ °C. An $f=50$ mm lens makes a $M=13\times$ magnified image of the near field onto an intermediate plane, which is then demagnified by a factor $1/28\times$ by imaging it with objectives onto the input tips of two optical fibers. The transverse correlations are measured by keeping detector 2 centered at $M\boldsymbol{\rho}_2=\mathbf{0}$ and moving detector 1 horizontally over $Mx_1=M|\boldsymbol{\rho}_1|$. To measure the longitudinal ($z$) dependence of the correlations, we move the crystal with a translation stage around the "object plane" of the lens . This will displace the near-field structure in the vicinity of the image plane. The on-axis phase mismatch $\varphi(T)$ can be adjusted by setting the temperature of the crystal. The derivative $d\varphi/dT \approx1.04$ K$^{-1}$ was calculated and checked experimentally [14]. The waist of the Gaussian detection modes, $w_d=80$ $\mu$m at the image plane and 6.7 $\mu$m at the crystal, was chosen to provide a good trade-off between resolution and detection efficiency.

Figure 2(a) shows the full spatial dependence of the coincidence counting rate $R_{\text{cc}}(\boldsymbol{\rho}_-,z) \propto |V_{\text{project}}(\boldsymbol{\rho}_-;z)|^2$ for the interesting phase mismatch $\varphi=+2.0\pm0.1$. The projections of the $\boldsymbol{\rho}_-=\mathbf{0}$ and $z=0$ curves are shown on the back and lateral planes, respectively. The single count rate ($\propto$ optical intensity) is practically constant over this scan, as indicated by the upper curves in the two projections (the full intensity surface is not shown). The experimental results are in perfect agreement with the theoretical prediction obtained from Eq. (4) and depicted as Fig. 2(b).

The three-dimensional reconstruction of the coincidence counting rate displays intriguing structures. For positive phase mismatch, as in Fig. 2, there are two well-pronounced peaks in the coincidence profile which are separated by the
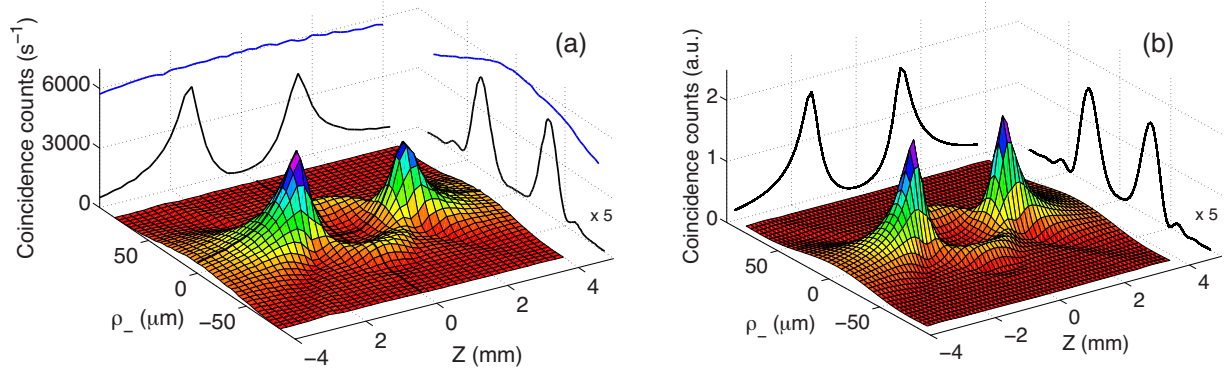


FIG. 2. (Color online) (a) Measured coincidence rate $R_{\text{cc}}(\boldsymbol{\rho}_-,z) \propto |V_{\text{project}}(\boldsymbol{\rho}_-;z)|^2$ at a phase mismatch $\varphi=2.0\pm0.1$. The intersections with the $\boldsymbol{\rho}-=\mathbf{0}$ and $z=0$ planes are projected on the back and lateral side of the plot. The transverse correlations for $z=0$ are amplified five times on the lateral plane. The upper (blue) curves represent similar projections of the single count rate of the scanning detector (not in scale; full intensity distribution not shown). (b) Theoretical results as predicted by Eq. (4). No fitting parameters are necessary.

imaging optical thickness of the crystal $L/n \approx 2.7$ mm. The physical origin of this structure can be understood as follows. The crystal acts as a longitudinally extended source of photon pairs. The phase-matching conditions determine the relative phase of photon pairs born at different planes within the pumped region. The final probability amplitude of detection is given by the sum of all contributions from many creation sites inside the crystal and propagated to the image plane. A fourth-order interference effect will lead then to the observed result. The change from an on-axis interference peak to an interference valley after free-space propagation also appears in the context of Fresnel diffraction. However, one must emphasize that the observed peculiar interference structure is only present in the fourth-order correlation function as the single count rates remain approximately constant during the scans.

It is possible to show that for points on-axis $\boldsymbol{\rho}_- = \mathbf{0}$ our mathematical description becomes identical to a classical expression used in nonlinear optics for the efficiency of second-harmonic generation in a medium pumped by a tightly focused Gaussian beam. The classical counterpart of our results has been predicted and observed a long time ago [7,8]. This is the experimental observation of a similar effect in the context of SPDC. By properly setting the phase-mismatch parameter $\varphi$ many of the longitudinal correlations presented in [7] can also be obtained with SPDC light.

The central part of Fig. 2 exhibits an almost total suppression of coincidence counts (but not of singles) for points on-axis. The observation of this on-axis minimum is an experimental proof of the quantum nature of the field and the presence of spatial antibunching. This statement is based on the work by Nogueira *et al.* [9], who showed that the fourth-order correlation function of any classical homogeneous field, where $\langle I(\boldsymbol{\rho}_1)I(\boldsymbol{\rho}_2)\rangle \propto R_{cc}(\boldsymbol{\rho}_1, \boldsymbol{\rho}_2)$ is a function of $\boldsymbol{\rho}_- = \boldsymbol{\rho}_1 - \boldsymbol{\rho}_2$ only, should obey a Cauchy-Schwarz-type inequality. For our correlation, which is homogeneous as $V(\boldsymbol{\rho}_-)$ depends only on $\boldsymbol{\rho}_-$, this classical inequality reads

$$|V(\boldsymbol{\rho}_-)|^2 \leq |V(\mathbf{0})|^2. \tag{5}$$

The violation of inequality (5) observed in Fig. 2 therefore implies that the generated two-photon field is nonclassical and spatially antibunched; the field is at the same time homogeneous and reveals destructive fourth-order interference for $\boldsymbol{\rho}_- = \mathbf{0}$ in the image plane. This is perhaps the simplest and most direct method up to date to observe spatial antibunching in the two-photon field.

By varying the phase mismatch $\varphi$ many different three-dimensional profiles can be obtained. As another example, Fig. 3 shows the spatial correlations measured for $\varphi = -5.2 \pm 0.1$. Notice the prominent ripples in the transverse correlations observed in the $z = 0$ plane. Both coincidence profiles in Figs. 2 and 3 are symmetric with respect to the $z = 0$ plane, as predicted by Eq. (3).

Since we have now a complete understanding of the structure of the two-photon field in the near-field regime, we can revisit previous works that were analyzed under certain approximations. In a recent experiment of Howell *et al.* [12] measurements of position correlations were used to violate separability criteria in a realization of the Einstein-Podolsky-
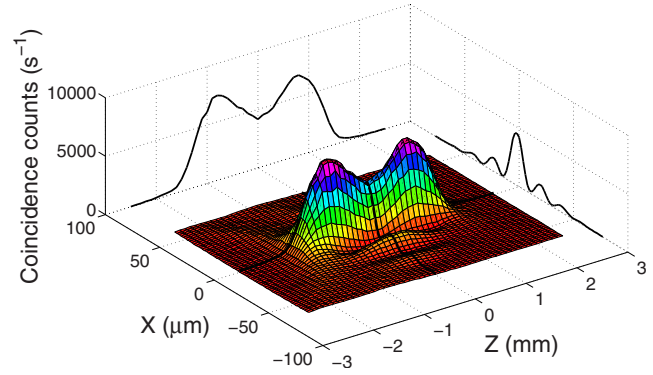


FIG. 3. (Color online) Measured coincidence rate $R_{cc}(\boldsymbol{\rho}_-, z) \propto |V_{\text{project}}(\boldsymbol{\rho}_-; z)|^2$ at a phase mismatch $\varphi = -5.2 \pm 0.1$. The intersections with the $\boldsymbol{\rho}- = \mathbf{0}$ and $z = 0$ planes are projected on the back and lateral sides of the plot.

Rosen (EPR) paradox. One of the key results was the measured conditional variance $(\Delta x_1|_{x_2})^2$, which was taken at a single plane in the near field. In Fig. 4 we show our measured transverse correlations at perfect phase matching ($\varphi = 0$), with the crystal facet imaged at the detection plane [Fig. 4(a)] and the center of the crystal [Fig. 4(b)]. The calculated variance $(\Delta x_1|_{x_2})^2$ for these two plots differs by 35%, implying that the variance product used to quantify the EPR paradox is not unique. On the other hand, it is well known that the amount of entanglement cannot change under free-space propagation. These differences are due to the fact that the considered uncertainty relations are based on intensity mea-
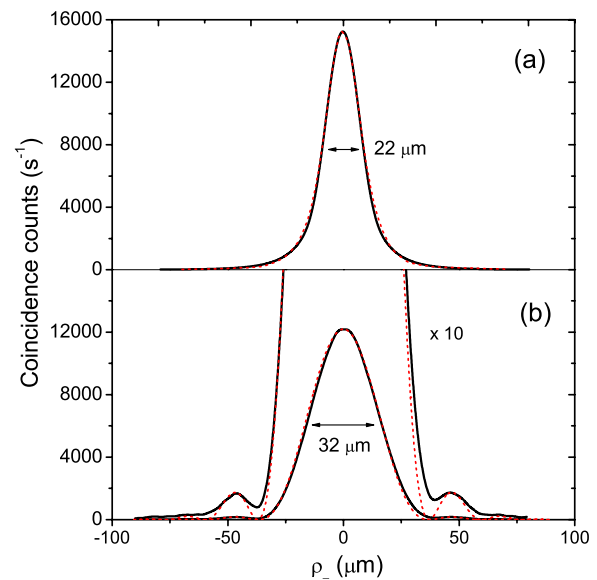


FIG. 4. (Color online) Transverse correlations close to perfect phase matching ($\varphi = 0.0 \pm 0.2$) for (a) the crystal facet imaged and (b) the center of the crystal imaged on the detection plane. The solid (black) curves are the experimental data, while the dashed (red) curves are theoretical predictions. The $10\times$ magnified plot shows the agreement between theory and experiment also at the side bumps. The indicated full width at half maximum (FWHM) of the curves varies with the focused plane. The ratio between the peak heights $\approx 1.25$.

surements, whereas entanglement can also exist in the phase of the two-photon field. In this way we provide experimental support to the proposed migration of entanglement in Hilbert space between amplitude and phase [15].

Note that one cannot interpret the results shown in Fig. 4 as the probability distribution of the "relative birthplace" of the photons [12] since the correlations obtained are a consequence of interference of photons generated at all possible sites in the crystal. This point can be strengthened by considering the observed spatial antibunching in Fig. 2, which is not in contradiction with the assumption of localized emission.

In conclusion, we have reported a complete experimental observation of the near-field structure in the two-photon field. Contrary to the predominant view in the literature, the exact form of the phase-matching function leads to striking observable effects, such as many complex and intriguing structures in the transverse correlations, longitudinal correla-

tions that resemble those observed in SHG with tightly focused beams, and a way of producing spatial antibunching. The fact that these correlations can be easily measured may open a window on experimental studies of continuous variable entanglement. First, it allows one to corroborate and compare different proposed entanglement measures [16–18] in the near-field regime. Additionally, issues such as the behavior of entanglement under propagation can be addressed. Finally, previous works that were analyzed under approximations regarding the near-field correlations in SPDC, e.g., realization of the EPR paradox [12], quantum optical lithography [3,4], and entanglement migration in Hilbert space [15], can now be revisited.

[1] T. B. Pittman, D. V. Strekalov, D. N. Klyshko, M. H. Rubin, A. V. Sergienko, and Y. H. Shih, Phys. Rev. A **53**, 2804 (1996).

[2] D. V. Strekalov, A. V. Sergienko, D. N. Klyshko, and Y. H. Shih, Phys. Rev. Lett. **74**, 3600 (1995).

[3] A. N. Boto *et al.*, Phys. Rev. Lett. **85**, 2733 (2000).

[4] M. D'Angelo, M. V. Chekhova, and Y. Shih, Phys. Rev. Lett. **87**, 013602 (2001).

[5] T. Yarnall, A. F. Abouraddy, B. E. A. Saleh, and M. C. Teich, Phys. Rev. Lett. **99**, 170408 (2007).

[6] C. H. Monken, P. H. Souto Ribeiro, and S. Pádua, Phys. Rev. A **57**, 3123 (1998).

[7] D. A. Kleinman and R. C. Miller, Phys. Rev. **148**, 302 (1966).

[8] G. D. Boyd and D. A. Kleinman, J. Appl. Phys. **39**, 3597 (1968).

[9] W. A. T. Nogueira, S. P. Walborn, S. Pádua, and C. H. Monken, Phys. Rev. Lett. **86**, 4009 (2001).

[10] D. P. Caetano and P. H. Souto Ribeiro, Phys. Rev. A **68**, 043806 (2003).

[11] M. D'Angelo, Y. H. Kim, S. P. Kulik, and Y. Shih, Phys. Rev. Lett. **92**, 233601 (2004).

[12] J. C. Howell, R. S. Bennink, S. J. Bentley, and R. W. Boyd, Phys. Rev. Lett. **92**, 210403 (2004).

[13] B. E. A. Saleh, A. F. Abouraddy, A. V. Sergienko, and M. C. Teich, Phys. Rev. A **62**, 043816 (2000).

[14] W. H. Peeters and M. P. van Exter, Opt. Express **16**, 7344 (2008).

[15] K. W. Chan, J. P. Torres, and J. H. Eberly, Phys. Rev. A **75**, 050101(R) (2007).

[16] S. Mancini, V. Giovannetti, D. Vitali, and P. Tombesi, Phys. Rev. Lett. **88**, 120401 (2002).

[17] C. K. Law and J. H. Eberly, Phys. Rev. Lett. **92**, 127903 (2004).

[18] M. V. Fedorov, M. A. Efremov, P. A. Volkov, and J. H. Eberly, J. Phys. B **39**, S467 (2006).